KSCE Journal of Civil Engineering
DOI 10.1007/s12205-024-0086-8

pISSN 1226-7988, eISSN 1976-3808
www.springer.com/12205

Structural Engineering

A Numerical Research on Dynamic Interaction of the Rubber Soil Foundation and Structure

Shan Lu[a], Gao Lin[b], Zhiyun Wang[a], Yi Ma[d], and Hengliang Zhao[c]

[a]School of Marine and Civil Engineering, Dalian Ocean University, Dalian 116023, China
[b]School of Hydraulic Engineering, Faculty of Infrastructure Engineering, Dalian University of Technology, Dalian 116024, China
[c]School of Civil Engineering, Shenyang Jianzhu University, Shenyang 110168, China
[d]Dalian Institute of Architecture Design & Research Co., Ltd., Dalian 116011, China

ARTICLE HISTORY

Received 3 February 2023
Revised 17 November 2023
Accepted 17 July 2024
Published Online 9 September 2024

KEYWORDS

Rubber soil
Soil-structure interaction
Seismic isolation
Wave propagation

ABSTRACT

This paper presents an innovative seismic isolation system for the structure and unbounded rubber soil. The dynamic interaction of the rubber soil and structure is considered. The rubber soil mixture is constituted by rubber particles and clay. The pollution problem of wast rubber is solved effectively. The rubber soil is firstly introduced into the ordinary unbounded foundation. According to the composite material theory and hybrid law, the rubber soil modulus formulation is derived by two-phase modulus innovatively. By employing the standard viscous boundary method, the radiation damping of unbounded rubber soil is considered. And then, the novel wave propagation equation of unbounded rubber soil is derived. Based on the cylindrical expansion wave and cut-off wave assumptions, the normal and tangential boundary condition equations are derived, respectively. The interaction force causing by earthquake on the rubber soil and structure is modeled. Numerical examples are presented to demonstrate the effectiveness and reliability of the proposed method for the rubber soil and structure interaction model. The seismic response of the rubber soil and structure system is discussed. Excellent seismic performance of rubber soil is confirmed. The influence of the rubber soil content and thickness are discussed in detail.

1. Introduction

The foundation isolation is a new type of active control technique to reduce the earthquake disaster. This interesting research is attracting more and more attention of engineers. In recently years, the rubber is widely applied in civil engineering (Moghaddas et al., 2016; Mohajerani et al., 2020; Sanchez, 2020; Tasalloti et al., 2020; Manohar and Anbazhagan, 2021). The rubber has the characteristics of low modulus, high elasticity and damping. Therefore, the energy consumption ability of the rubber particles and soil mixture (rubber soil) has been significantly improved. It is very meaningful to study the seismic response of rubber soil.

With the automotive industry boom, the disposal of waste rubber causes the serious environmental pollution. Many researchers have developed various treatment methods to overcome this pollution problem. Therefore, the reasonable treatment of waste rubber is a urgent problem. The rubber products are processed into rubber particles, and then they are applied in the asphalt, concrete and soil in the civil engineering. Not only the performance of civil engineering materials has been improved, but also a great number of waste rubber products have been consumed. In order to investigate the shear modulus and damping ratio of rubber sand mixtures, the cyclic triaxial tests with different rubber weight were conducted (Fakharian and Ahmad, 2021). Enquan and Qiong (2019) obtained the shear strength and liquefaction potential of saturated rubber-sand mixtures by the experimental investigation. The well-designed layer of sand and rubber sand mixed as base isolater was studied by the shake table tests (Bandyopadhyay et al., 2015). The rubber soil mixtures is an innovative concept in geotechnical seismic isolation system. It has attracted considerable research interest on its performance at both system and material levels, since it was first proposed over a decade ago (Tsang and Pitilakis, 2019). Whereafter, the performance of seismic isolation system of structure and rubber soil mixtures was tested (Tsang et al., 2021). The

CORRESPONDENCE Zhiyun Wang wangzhiyun1980@163.com School of Marine and Civil Engineering, Dalian Ocean University, Dalian 116023, China

isolation mechanism and effectiveness of rubber soil isolation system were confirmed by experimental research (Pistolas et al., 2020). Results revealed that the seismic response of rubber soil foundation was significantly reduced, and the re-use of scrap tires can reduce environmental pollution. A sand-rubber deformable granular layer as a low-cost seismic isolation system was investigated experimentally by Tsiavos et al. (2019). The experimental results showed that the seismic performance of sand-rubber was well. And then, the excellent seismic performance of gravel-rubber mixture was analyzed by a large-scale experiment (Pitilakis et al., 2021). Nanda et al. (2018) employed the numerical method to analyze the seismic response of buildings with rubber-soil mixture as foundation isolation. Brunet et al. (2016) modeled a structure underlain by strongly nonlinear rubber soil. The results showed that rubber-soil mixtures played an very important role in the seismic isolation system. The characterization of the sand-rubber tyre shreds mixtures was analyzed by Madhusudhan et al. (2019), the satisfactory dynamic properties was proved. The strength and deformation of sand-rubber mixtures were obtained by the direct shear tests (Wang et al., 2018; Rouhanifar et al., 2020).

The interaction of soil and structure has always been a worthwhile research topic. This research direction has attracted many scholars (Pitilakis et al., 2015; Dhanya et al., 2020; Pistolas et al., 2020). The soil-structure interaction is a prominent issue in the dynamic analysis of large structures, such as the dam, high-rise buildings, nuclear reactors, offshore wind plants and so on. Numerous research works have been performed to obtain the accurate and easy-to-implement soil-structure interaction models (Josifovski, 2016; Yuan et al., 2019; Olia and Perić, 2021). One of the biggest challenges is how to model the radiation damping of unbounded domain. The building seismic response by considering the soil-structure interaction was evaluated (Arboleda-Monsalve et al., 2020). Abdulrasool et al. (2020) presented the semi-infinite extension theory to simulate the unbounded domain. And the absorbing layer was used to create boundaries. This boundaries can significantly decrease the wave reflect into bounded area.

With the continuous development of theoretical research, numerous scholars have employed numerical methods to analyze the dynamic interaction of complex unbounded domain. The foundation boundary conditions and the seismic wave input have undergone extensive research. The perfectly matched layers around the finite region of interest local transmitting boundaries for wave propagation problems was used to model unbounded domain (Fontara et al., 2018). The restrictions of traditional wave input methods on the type of artificial boundaries was released (Liu et al., 2019). Additionally, an accurate absorbing boundary condition for multilayer fluid-saturated porous medium was applied (Zhang et al., 2020). The numerical stability analysis for the dynamic soil-structure interactions using viscoelastic artificial boundary method was determined (Li et al., 2020). The seismic analysis of soil structure dynamic interaction based on the substructure of artificial boundaries was solved (Jingbo et al., 2018). A direct FEM for nonlinear earthquake analysis of 2D dam-water-foundation rock systems was presented (Løkke and Chopra, 2018). Furthermore, semi-unbounded foundation-rock and fluid domains were modeled using standard viscous-damper absorbing boundaries. The dynamic analysis of the artificial boundary condition coupling with 3D FEM model for unbounded media was also found (Zhao et al., 2019). In the analysis of soil-structure seismic response or the near-field seismic wave propagation, the viscoelastic artificial boundary was applied to transform the unbounded domain problem into a bounded domain problem (Li et al., 2020). They proposed a stability analysis method for the explicit time-domain stepwise integration algorithm when using the two-dimensional viscoelastic artificial boundary elements. At present, there are no appropriate analysis methods and research results to determine the layered rubber-soil dynamic interaction. The rubber soil interaction has become a cutting-edge topic for further research.

In this study, we investigated the dynamic response of the layered rubber-soil interaction by using the two-dimensional viscoelastic artificial boundary method. In Section 2, the composite material theory of rubber soil is introduced. In Section 3, the derivation of the two-dimensional viscoelastic boundary for unbounded domain is considered. In Section 4, the earthquake input method by two-dimensional viscoelastic boundary is established. The general form of the equivalent earthquake load is given. In Section 5, the dynamic properties of the layered rubber-soil foundation are analyzed by numerical examples. The influences of rubber-soil depth, thickness, rubber powder content are discussed. In Section 6, the earthquake response study of the dam and rubber-soil foundation model is developed. Conclusion remarks are stated in Section 7.

2. Composite Material Theory of the Rubber Soil Modulus

The elastic modulus is an important mechanical property of rubber soil. This research has emphasizing significance in engineering applications. The rubber soil can be regarded as a two-phase composite material consisting of rubber and soil. Based on the composite material theory, the mixture material modulus can be obtained through the two-phase modulus by hybrid law. The derivation procedure of rubber soil modulus is similar to the process in reference (Wang, 2019). For the sake of simplicity, a concise summary of the necessary equations is presented in this section.

The hybrid law primarily relies on two assumptions, the Voigt equal strain assumption and Reuss equal stress assumption. In the first assumption, the external load acting on the composite material is divided equally between the two constituent materials. And, the corresponding strains of two materials are equal to those of the composite material. For the rubber soil, rubber and soil, the strains are as follow $\varepsilon_{rs} = \varepsilon_r = \varepsilon_s$. where symbols rs, r and s represent the rubber soil, rubber and soil, respectively. Because the external load is borne by the rubber and soil, then

$$\sigma_{rs} A_{rs} = \sigma_r A_r + \sigma_s A_s \ , \tag{1}$$

where A_r, A_s and A_{rs} are the area in unit length for the rubber, soil and rubber soil. σ_r, σ_s and σ_{rs} are the stress for the rubber, soil and rubber soil.

According to the strain equivalent condition, Eq. (1) is divided by the correlation strain yield,

$$\frac{\sigma_{rs} A_{rs}}{\varepsilon_{rs}} = \frac{\sigma_r A_r}{\varepsilon_r} + \frac{\sigma_s A_s}{\varepsilon_s} , \tag{2}$$

where ε_r, ε_s and ε_{rs} are the strain for rubber, soil and rubber soil, respectively.

Then, the Voigt elastic modulus is obtained.

$$E_{rs} = \xi_r E_r + \xi_s E_s , \tag{3}$$

where E_{rs}, E_r and E_s are the elastic modulus of rubber soil, rubber and soil, respectively. ξ_r and ξ_s are the volume percentages of rubber and soil, and $\xi_r + \xi_s = 1$.

In the Reuss equal stress assumption, two-phase materials have equal stress under external load $\sigma_{rs} = \sigma_r = \sigma_s$. Consequently, the composite material deformation is composed by the two-phase deformation.

$$\varepsilon_{rs} l_{rs} = \varepsilon_r l_r + \varepsilon_s l_s , \tag{4}$$

in which, l_r, l_s and l_{rs} are the original length in under unit area for rubber, soil and rubber soil, respectively.

According to the stress equivalent condition, Eq. (4) is divided by the correlation stress yield,

$$\frac{\varepsilon_{rs} l_{rs}}{\sigma_{rs}} = \frac{\varepsilon_r l_r}{\sigma_r} + \frac{\varepsilon_s l_s}{\sigma_s} . \tag{5}$$

Hence, the Reuss elastic modulus is expressed as

$$E_{rs} = \left(\frac{\xi_r}{E_r} + \frac{\xi_s}{E_s} \right)^{-1} . \tag{6}$$

Only considering the elastic deformation of the rubber soil, the strain energy can be defined as

$$U = \frac{1}{2} E_{rs} \varepsilon_{rs}^2 V , \tag{7}$$

with V is volume, U is strain energy.

We assume that there is a permissible stress field within rubber soil. The inside equilibrium condition and boundary condition are both satisfied. And U_σ is defined as the strain energy of the permissible stress field. Basing on the linear elastic assumption, the strain energy is equal to residual energy. Then, according to the minimum residual energy principle yields $U_\sigma \geq U$, where U is the strain energy corresponding to the real stress field.

$$U_\sigma = \frac{1}{2} \int \frac{\sigma_{rs}^2}{E_{rs}} dV = \frac{1}{2} \sigma_{rs}^2 \int_V \frac{dV}{E_{rs}} , \tag{8}$$

where U_σ is the strain energy of the permissible stress field.

The integration range contains the volume of rubber and soil, then Eq. (8) can be expressed as

$$U_\sigma = \frac{1}{2} \sigma_{rs}^2 \left(\int_{\xi_s} \frac{dV}{E_s} + \int_{\xi_r} \frac{dV}{E_r} \right) . \tag{9}$$

Further simplification, the result is that

$$U_\sigma = \frac{1}{2} \sigma_{rs}^2 \left(\frac{\xi_s}{E_s} + \frac{\xi_r}{E_r} \right) V . \tag{10}$$

According to Eqs. (7) and (10), it can be found that the Reuss modulus E_{rs} is the lower limit of rubber soil modulus. Basing on the minimum energy principle, the strain energy U_ε is bigger than the strain energy of the real strain states, $U_\varepsilon \leq U$.

$$U_\varepsilon = \frac{\varepsilon_{rs}^2}{2} \left[\frac{1 - \nu_s - 4\nu\nu_{rs} + 2\nu^2}{(1 - 2\nu_{rs})(1 + \nu_{rs})} E_{rs} \xi_{rs} + \frac{1 - \nu_r - 4\nu\nu_r + 2\nu^2}{(1 - 2\nu_r)(1 + \nu_r)} E_r \xi_r \right] V , \tag{11}$$

where U_ε is strain energy, ν_r, ν_s and ν_{rs} are the poisson ratio of rubber, soil and rubber soil. ν is an unknown constant.

Considering Eqs. (7) and (11), yield

$$E_{rs} \leq \frac{1 - \nu_s - 4\nu\nu_s + 2\nu^2}{(1 - 2\nu_s)(1 + \nu_s)} E_s \xi_s + \frac{1 - \nu_r - 4\nu\nu_r + 2\nu^2}{(1 - 2\nu_r)(1 + \nu_r)} E_r \xi_r . \tag{12}$$

The unknown constant ν can be obtained from the limit value of strain energy U_ε.

$$\frac{\partial U_g}{\partial \nu} = 0 , \tag{13}$$

$$\nu = \frac{\nu_s (1 - 2\nu_r)(1 + \nu_r) E_s \xi_s + \nu_r (1 - 2\nu_s)(1 + \nu_s) E_r \xi_r}{(1 + 2\nu_r)(1 + \nu_r) E_s \xi_s + (1 - 2\nu_s)(1 + \nu_s) E_r \xi_r} , \tag{14}$$

when $\nu_s = \nu_r$, the unknown constant can be expressed as

$$\nu = \nu_s = \nu_r . \tag{15}$$

Substituting Eqs. (14) and (15) into Eq. (12), the upper limit of E_{rs} can be defined as

$$E_{rs} \leq E_s \xi_s + E_r \xi_r . \tag{16}$$

According to the composite material theory, the rubber soil modulus is between the upper and lower limits. Hence, combining the test data in Reference Zhou (2009), the expression of rubber soil modulus is recommended as follow.

$$E_{rs} = (1 - k)(\xi E_r + \xi_s E_s) + k \left(\frac{\xi}{E_r} + \frac{\xi_s}{E_s} \right)^{-1} , \tag{17}$$

where k is a adjustment coefficient ($k < 1$)

3. The Theory and Realization of the Two-Dimensional Viscoelastic Boundary

The viscoelastic boundary method is an effective approach to model unbounded domain problem. In this section, the derivation process of the two-dimensional viscoelastic boundary is introduced. Assuming the wave propagation medium on the boundary is an anisotropic uniform linear elastic material. Basing on the cylindrical expansion wave and cut-off wave assumptions of the outer wave, the normal and tangential boundary condition equations in plane are derived, respectively.

3.1 Summary of the Normal Viscoelastic Boundary

3.1.1 The General Solution of the Wave Equation

Because the propagation of a cylindrical expansion wave in the medium, the microelement in the medium is subjected to external load. According to the equilibrium condition, the radial equilibrium equation can be given as

$$\rho\frac{\partial^2 u}{\partial t^2}=\frac{\partial\sigma_r}{\partial r}+\frac{\sigma_r-\sigma_\theta}{r}\ , \tag{18}$$

where ρ is material density, u is displacement, σ_r and σ_θ are the stresses in r-direction and θ-direction, respectively. Then, according to the physical and geometric equilibrium equations,

$$\sigma_\theta=\lambda\varepsilon_r+(2G+\lambda)\varepsilon_\theta\ , \tag{19}$$

$$\sigma_r=(2G+\lambda)\varepsilon_r+\lambda\varepsilon_\theta\ , \tag{20}$$

$$\varepsilon_\theta=\frac{u}{r}\ , \tag{21}$$

$$\varepsilon_r=\frac{\partial u}{\partial r}\ , \tag{22}$$

where ε_r and ε_θ are the strains in r-direction and θ-direction, respectively. G is shear modulus, λ is lame's constant, r is radial coordinate, u is displacement.

The wave equation can be obtained.

$$\frac{\partial^2 u}{\partial t^2}=\frac{2G+\lambda}{\rho}\left(\frac{\partial^2 u}{\partial r^2}+\frac{1}{r}\frac{\partial u}{\partial r}-\frac{u}{r^2}\right), \tag{23}$$

where, the Lame's constant $\lambda=\frac{\mu E}{(1+\mu)(1-2\mu)}$, is Poisson's ratio μ and E is Young's modulus. For the sake of simplifying, introducing the displacement potential function ϕ, then the displacement can be expressed as $u=\frac{\partial\phi}{\partial r}$. The relationship of displacement and potential function is applied to the wave Eq. (23).

$$\frac{\partial}{\partial r}\frac{\partial^2\phi}{\partial t^2}=\frac{2G+\lambda}{\rho}\frac{\partial}{\partial r}\left(\frac{\partial^2\phi}{\partial r^2}+\frac{1}{r}\frac{\partial\phi}{\partial r}\right), \tag{24}$$

where ϕ is displacement potential function.

Integrating Eq. (24) with radial coordinate r,

$$\frac{\partial^2\phi}{\partial t^2}=c_p^2\left(\frac{\partial^2\phi}{\partial r^2}+\frac{1}{r}\frac{\partial\phi}{\partial r}\right), \tag{25}$$

in which, $c_p=\sqrt{\frac{2G+\lambda}{\rho}}$ is expansion wave velocity.

The exact expression for cylindrical wave cannot be obtained, but the approximate solution can be expressed as

$$\phi(r,t)=\frac{1}{\sqrt{r}}f\left(\frac{r}{c_p}-t\right), \tag{26}$$

where f is function representing wave shape. Then, the displacement can be obtained by integration with r.

$$u(r,t)=\frac{\partial\phi}{\partial r}=-\frac{1}{2r^{\frac{3}{2}}}f+\frac{1}{c_p\sqrt{r}}f' \tag{27}$$

According to Eq. (20), the radial stress σ_r can be given as

$$\sigma_r=(2G+\lambda)(\varepsilon_r+\varepsilon_\theta)-2G\varepsilon_\theta\ . \tag{28}$$

Combining Eqs. (21) and (22), and considering Eq. (25)

$$\varepsilon_r+\varepsilon_\theta=-\frac{\partial u}{\partial r}-\frac{u}{r}=-\frac{\partial^2\phi}{\partial r^2}-\frac{1}{r}\frac{\partial\phi}{\partial r}=-\frac{1}{c_p^2}\frac{\partial^2\phi}{\partial t^2} \tag{29}$$

Substituting Eqs. (27) into Eq. (21), the circumferential strain can be expressed as

$$\varepsilon_\theta=-\frac{u}{r}=\frac{1}{2r^{\frac{5}{2}}}f-\frac{1}{c_p r^{\frac{3}{2}}}f'\ . \tag{30}$$

Substituting Eqs. (29) and (30) into Eq. (28), the radial stress is obtained as

$$\sigma_r=(2G+\lambda)\left(-\frac{1}{c_p^2}\frac{\partial^2\phi}{\partial t^2}\right)-2G\left(\frac{1}{2r^{\frac{5}{2}}}f-\frac{1}{c_p r^{\frac{3}{2}}}f'\right). \tag{31}$$

According to Eq. (27), the differentiation of displacement u with respect t can be expressed as

$$\frac{\partial u}{\partial t}(r,t)=\frac{-1}{2r^{\frac{3}{2}}}f'(r,t)-\frac{1}{c_p\sqrt{r}}f'(r,t)\ , \tag{32}$$

$$\frac{\partial^2 u}{\partial t^2}(r,t)=\frac{-1}{2r^{\frac{3}{2}}}f''(r,t)+\frac{1}{c_p\sqrt{r}}f''(r,t)\ . \tag{33}$$

Second time derivative of the potential in Eq. (26) yields

$$\frac{\partial^2\phi}{\partial t^2}(r,t)=\frac{1}{\sqrt{r}}f''(r-t)\ . \tag{34}$$

Substituting Eqs. (34) into (31), the radial stress at boundary can be founded

$$\sigma_r = (2G+\lambda)\left(-\frac{1}{c_p^2\sqrt{r}}f''\right) - 2G\left(\frac{1}{2r^{\frac{5}{2}}}f - \frac{1}{c_p r^{\frac{3}{2}}}f'\right)$$
$$= \frac{2G}{r}\left(u(r,t) - \frac{(2G+\lambda)r}{2G}\frac{1}{c_p^2\sqrt{r}}f''\right). \tag{35}$$

Differentiating Eq. (36) with respect to time t

$$\frac{\partial\sigma_r}{\partial t}(r,t) = \frac{2G}{r}\left(\frac{\partial u}{\partial t}(r,t) + \frac{(2G+\lambda)r}{2G}\frac{1}{c_p^2\sqrt{r}}f'''\right). \tag{36}$$

According to Eqs. (35) and (36), the unknown function f can be removed, and the only variable quantity is r.

$$\sigma_r + \frac{2r}{c_p}\frac{\partial\sigma_r}{\partial t}(r,t) = \frac{2G}{r}\left(u + \frac{2r}{c_p}\frac{\partial u}{\partial t} + \frac{r^2}{c_p^2}\frac{2G+\lambda}{G}\frac{\partial^2 u}{\partial t^2}\right) \tag{37}$$

Equation (37) is independent of the wave form function f. The boundary condition merely approximates the influence of unbounded domain. Eq. (37) includes the time derivative of the boundary stress. The boundary differential equation can be numerically solved in finite element analysis technology by integrating Eq. (37) over time. For the sake of more conveniently, the spring-dashpot-mass model proves to be more meaningful.

3.1.2 Equivalent Normal Boundary Physical Element

The normal stress boundary condition is modeled by the spring-damping-mass element. The mechanic model is shown in Fig. 1. The equations of motion for model are formulated as

$$ku_1 + c(\dot{u}_1 - \dot{u}_2) = f_1\,, \tag{38}$$

$$m\ddot{u}_2 + c(\dot{u}_2 - \dot{u}_1) = 0\,, \tag{39}$$

where k is stiffness, m is mass, c is damp. u_1 and u_2 are the displacement of two freedom degrees. f_1 is the external force applying at the first freedom degree.

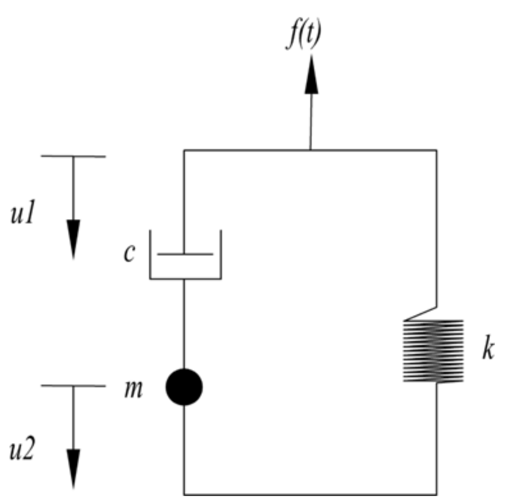

Fig. 1. Mechanical Model of Physical Component as the Radial Boundary

According to Eq. (38) and differentiating with respect to time yield

$$\ddot{u}_2 = \frac{1}{c}(k\dot{u}_1 + c\ddot{u}_1 - \dot{f}_1)\,. \tag{40}$$

Substituting Eq. (40) into Eq. (39)

$$f_1 + \frac{m}{c}\dot{f}_1 = k(u_1 + \frac{m}{c}\dot{u}_1 + \frac{m}{k}\ddot{u}_1) \tag{41}$$

By combining Eqs. (37) and (41), the equivalent distributed stiffness, damping and mass are expressed as

$$m = 2\rho r\,,\ c = \rho c_p\,,\ k = \frac{2G}{r}\,, \tag{42}$$

where ρ is density.

3.2 Summary of the Tangential Viscoelastic Boundary

3.2.1 The General Solution of the Wave Equation

Similar to the normal boundary derivation above, the equilibrium equation can be given as

$$\rho\frac{\partial^2 v}{\partial t^2} = \frac{\partial\tau}{\partial r} + \frac{2\tau}{r}\,, \tag{43}$$

where τ is shear stress. Then, according to the physical and geometric Eqs. (44) and (45), the wave equation can be given in Eq. (46).

$$\gamma = \frac{\partial v}{\partial r} + \frac{v}{r}\,, \tag{44}$$

$$\tau = G\gamma\,, \tag{45}$$

$$\frac{\partial^2 v}{\partial t^2} = \frac{G}{\rho}\left(\frac{\partial^2 v}{\partial r^2} + \frac{1}{r}\frac{\partial v}{\partial r} - \frac{v}{r^2}\right), \tag{46}$$

where γ is shearing strain. Introducing potential function ψ, then the vertical displacement can be expressed as $v = \frac{\partial\psi}{\partial r}$. The relationship of displacement and potential function is applied to the wave Eq. (46).

$$\frac{\partial}{\partial r}\frac{\partial^2\psi}{\partial t^2} = \frac{G}{\rho}\frac{\partial}{\partial r}\left(\frac{\partial^2\psi}{\partial r^2} + \frac{1}{r}\frac{\partial\psi}{\partial r}\right). \tag{47}$$

Integrating Eq. (47) with r,

$$\frac{\partial^2\psi}{\partial t^2} = c_s^2\left(\frac{\partial^2\psi}{\partial r^2} + \frac{1}{r}\frac{\partial\psi}{\partial r}\right), \tag{48}$$

where $c_s = \sqrt{\frac{G}{\rho}}$ is the shear wave velocity.

Similar to the above solution procedure, the approximate solution ψ can be obtained by solving Eq. (48).

$$\psi(r,t)=\frac{1}{\sqrt{r}}f\left(\frac{r}{c_s}-t\right) \tag{49}$$

According to the relationship $v=\frac{\partial\psi}{\partial r}$, the equation is integrated with r.

$$v(r,t)=-\frac{1}{2}r^{-\frac{3}{2}}f+\frac{1}{c_s}r^{-\frac{1}{2}}f' \tag{50}$$

Then, the shear velocity and acceleration are expressed as

$$\frac{\partial v}{\partial t}(r,t)=-\frac{1}{2}r^{-\frac{3}{2}}f'+\frac{1}{c_s}r^{-\frac{1}{2}}f'' , \tag{51}$$

$$\frac{\partial^2 v}{\partial t^2}(r,t)=-\frac{1}{2}r^{-\frac{3}{2}}f''+\frac{1}{c_s}r^{-\frac{1}{2}}f''' . \tag{52}$$

According to Eqs. (51) and (52), the unknown function f can be removed, and the only variable quantity is r.

$$\tau+\frac{2r}{c_s}\frac{\partial\tau}{\partial t}=-\frac{5G}{2r}\left(v+\frac{8r}{5c_s}\frac{\partial v}{\partial t}+\frac{4r^2}{5c_s^2}\frac{\partial^2 v}{\partial t^2}\right) \tag{53}$$

3.2.2 Equivalent Tangential Boundary Physical Element

The tangential stress boundary condition is represented by using the spring-damping-mass element. Its mechanical model is shown in Fig. 1.

According to the model in Fig. 2, the dynamic equilibrium differential equation of mechanical model can be given as

$$kv_1+c(\dot{v}_1-\dot{v}_2)=-f(t) , \tag{54}$$

$$m\ddot{v}_2+c(\dot{v}_2-\dot{v}_1)=0 . \tag{55}$$

Then

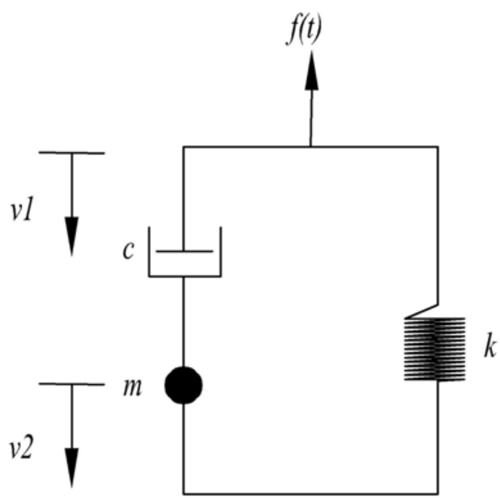

Fig. 2. Mechanical Model of Physical Component as the Tangential Boundary

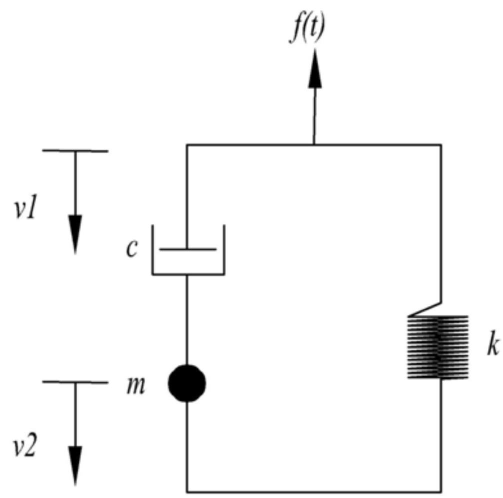

Fig. 3. Combine 14 Spring Damping Unit

$$f+\frac{m}{c}f'=-kv_1-\frac{mk}{c}\dot{v}_1-m\ddot{v}_1 . \tag{56}$$

Comparing with Eq. (53), the coefficients can be expressed as

$$k=\frac{2G}{\gamma} , \quad c=\rho c_s , \quad m=\frac{2Gr}{c_s^2} . \tag{57}$$

3.3 Expression of the Viscoelastic Boundary Condition

In this paper, the unbounded domain is modeled by using the viscoelastic boundary. Simulations of viscoelastic boundary can be easily implemented by combine 14 element in the finite element analysis, as shown in Fig. 3. In order tor model the radiation damping of unbounded domain, the normal and tangential spring-dampers are applied to the bounded domain boundaries, respectively. Moreover, the spring and damping coefficients are given as

$$K=\alpha\frac{G}{r}\sum_{i=1}^{l}A_i , \tag{58}$$

$$C=\rho c\sum_{i=1}^{l}A_i , \tag{59}$$

in which, K is equivalent stiffness, C is equivalent damp. r is the radiation radius of the scattering source to the boundary node. G is boundary shear stiffness. c is a general designation of wave speed, c_p and c_s are P or S wave speed for normal and tangential viscoelastic boundary, respectively. α is the coefficient in different direction boundaries, for in-plane case $\alpha=2.0$, for out-plane case $\alpha=0.5$. $\sum_{i=1}^{l}A_i$ is element line-area.

3.4 Earthquake Input Method Basing on the Viscoelastic Boundary

3.4.1 General Expression of the Equivalent Load

In this paper, the earthquake equivalent load on viscoelastic boundary

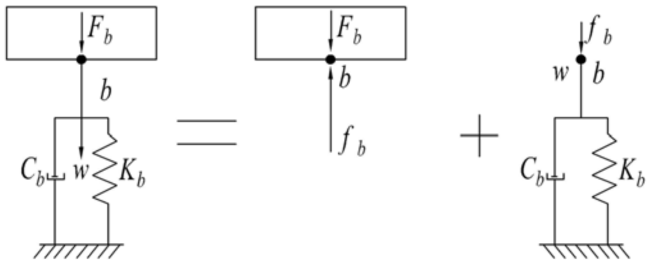

Fig. 4. Schematic Diagram of Artificial Boundary Stress Input in Viscoelasticity

is applied to model the structure-foundation interaction. The schematic diagram of stress input at viscoelastic boundary is given in Fig. 4. Based on the hypothesis that scattering wave can be fully absorbed by the viscoelastic boundary, the earthquake wave is converted into equivalent load acting on the boundary nodes. The treatment is currently more popular. The equivalent load is expressed as

$$F_b = R_b + C_b\dot{u} + K_b u\,, \tag{60}$$

where R_b is the interaction force between the unbounded and bounded domains. It contains the common action of incident wave, reflection wave and scattering wave. K_b is boundary stiffness. C_b is additional damping. F_b is boundary equivalent load.

3.4.2 The Specific Expression of Equivalent Load for Two Dimensional Model

For the two dimensional plane problem, the stress state of microelement can be obtained by means of elastic mechanics. Its geometric and physical equations are given as

$$\varepsilon_x = \frac{\partial u}{\partial x} \quad \varepsilon_y = \frac{\partial v}{\partial y} \quad \gamma_{xy} = \frac{\partial u}{\partial x} + \frac{\partial v}{\partial y}\,, \tag{61}$$

$$\begin{bmatrix}\sigma_x\\ \sigma_y\\ \tau_{xy}\end{bmatrix} = \begin{bmatrix}\lambda+2G & \lambda & 0\\ \lambda & \lambda+2G & 0\\ 0 & 0 & G\end{bmatrix}\cdot\begin{bmatrix}\varepsilon_x\\ \varepsilon_y\\ \gamma_{xy}\end{bmatrix}, \tag{62}$$

where ε_x, ε_y and γ_{xy} are the strains. σ_x, σ_y and τ_{xy} are the stresses.

According to Eq. (60), the specific expression of equivalent load for the in-plane problem can be obtained. For nodes on the bottom boundary, the equivalent load is denoted by

$$\begin{cases} F_h = k_t u + c_t\dot{u} - \tau_{xy}\sum\limits_{i=1}^{l} A_i \\ F_v = k_n v + c_t\dot{v} - \sigma_y\sum\limits_{i=1}^{l} A_i\,, \end{cases} \tag{63}$$

in which, F_h is the horizontal equivalent load, F_v is the vertical equivalent load. u and $\dot{u}$ are the horizontal velocity and acceleration. v and $\dot{v}$ are the vertical velocity and acceleration. σ_x, σ_y, τ_{xy} and τ_{yx} are the normal and tangential boundary stresses. k_n and k_t are the normal and tangential boundary spring coefficients. c_n and c_t are the normal and tangential boundary damping coefficients.

For the nodes on left boundary,

$$\begin{cases} F_h = k_n u + c_n\dot{u} - \sigma_x\sum\limits_{i=1}^{l} A_i \\ F_v = k_t v + c_t\dot{v} - \tau_{xy}\sum\limits_{i=1}^{l} A_i\,. \end{cases} \tag{64}$$

For the nodes on right boundary,

$$\begin{cases} F_h = k_n u + c_n\dot{u} - \sigma_x\sum\limits_{i=1}^{l} A_i \\ F_v = k_t v + c_t\dot{v} + \tau_{xy}\sum\limits_{i=1}^{l} A_i\,. \end{cases} \tag{65}$$

4. Dynamic Interaction of Rubber Soil and Structure

The dynamic interaction of two-dimensional rubber soil and structure is analyzed in this section. The viscoelastic artificial boundary is applied to simulate the radiative damping of unbounded rubber soil. Therefore, the refraction and scattering of wave in the unbounded rubber soil can be simulated accurately. The primary goal of this paper is to reveal a novel method which is suitable for the dynamic analysis of unbounded rubber soil. To illustrate the accuracy and wide applicability of proposed method, five numerical examples are investigated. In section 4.1, the accuracy of proposed method is verified by a unbounded soil model. By comparing with the theoretical solutions and extended finite element solutions, the accuracy of the proposed method is demonstrated. In section 4.2, the dynamic response of the layered rubber soil model is addressed. The effect of rubber soil depth is considered. In section 4.3, the earthquake response of gravity dam model is analyzed. The comparison study between the rubber soil and clay models is shown. In section 4.4, the influence of rubber content on the foundation earthquake response is analyzed. In section 4.5, the influence of rubber soil thickness is investigated.

4.1 Dynamic Analyze of Unbounded Soil

The numerical example is presented in this section to demonstrate the accuracy and efficiency of proposed method. A semi-infinite soil layer with free-surface is shown in Fig. 5. The semi-infinite soil is divided into bounded domain and unbounded domain. The geometry sizes of bounded domain are given as: the width L = 200 m, thickness H = 100 m. And the soil properties are: shear modulus $G = 5\times10^8$ Pa, poisson's ratio $\nu = 0.25$ and mass density ρ = 2,000 kg/m^3. As mentioned above, the viscous-spring boundary is used to model the unbounded domain, and the normal and shear boundary parameters (in plane) are $\alpha_n = 0.5$, $\alpha_t = 0.5$, respectively.

In order to demonstrate the accuracy of proposed method, the reference solution (Zhou, 2009) and the approximate theoretical solution (extended finite element solution) are selected, and the model and mesh sizes are the same as mentioning in reference. The bounded domain is discretized by eight-node finite elements

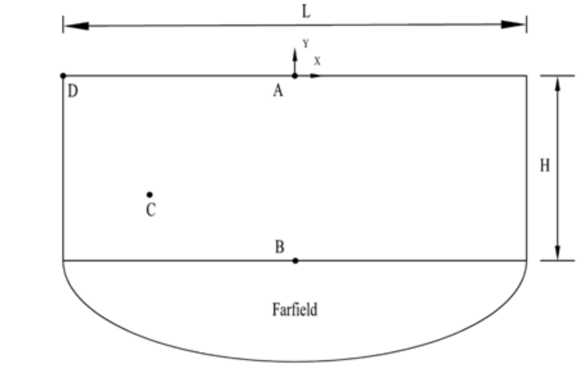

(a)

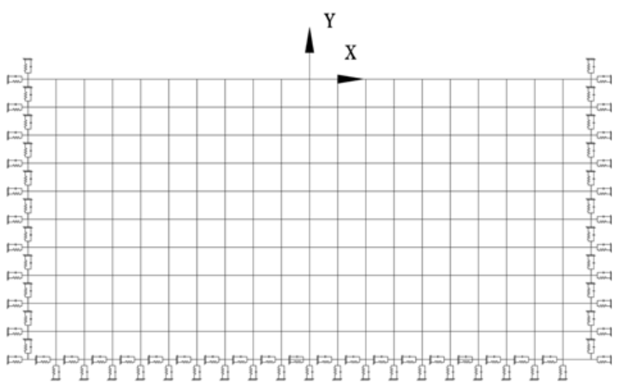

(b)

Fig. 5. The Unbounded Soil Model: (a) Calculation Diagram of Unbounded Soil Model, (b) Viscoelastic Boundary Model

Table 1. Observation Point Coordinates

Node	A	B	C	D
Coordinate	(0,0)	(0, -100 m)	(-60 m, -60 m)	(-100 m, 0)

with 10 m × 10 m mesh density.

As shown in Fig. 5, a vertical dynamic force pulse $P(t)$ acts on point A. Three observation points are selected the same as the reference (Zhou, 2009). The time step Δt is chosen as 0.01s, and the total acting time is chosen as 1.2s. Expression of the force $F(t)$ in time domain is as follow:

$$F(t)=\begin{cases}5\times10^4\sin(10\pi t) & t\le 0.2s\\ 0 & t>0.2s\end{cases}. \tag{66}$$

The vertical displacement responses of points B, C and D are evaluated in Fig. 6. Comparing with the reference solution and extended finite element solution, it is noted that the proposed method can achieve excellent accuracy. For $t<0.4s$, the proposed solutions are consistent with the reference and theoretical solutions. For $0.4s\le t\le 0.8s$, the displacement trends are more closer to the actual wave motion effect. The displacement amplitude decreases gradually with the energy decay. For $t\ge 0.8s$, the displacement amplitude changes are insignificant. This is because the energy decays with the external force decaying. From the figures, the displacement oscillatory behaviors of proposed method is significantly smaller than those of the other two reference solutions. The error can be accepted in reasonable range, and the error gradually decreases with time increases. Therefore, the proposed

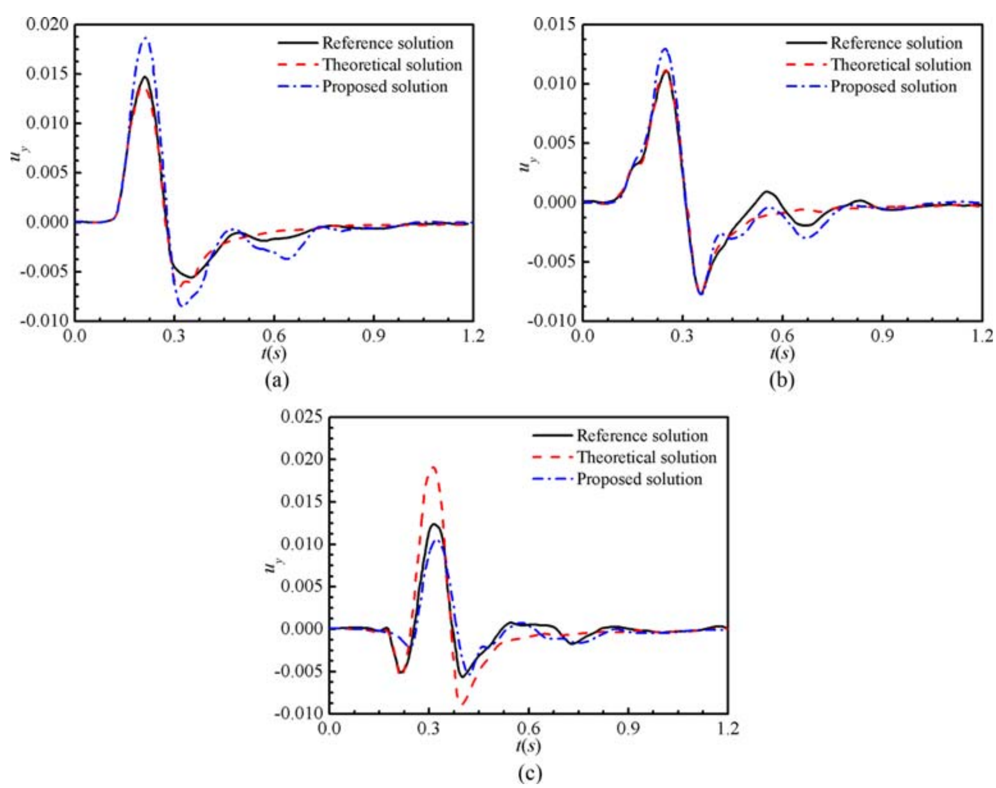

Fig. 6. Vertical Displacements of Points B, C and D: (a) Point B, (b) Point C, (c) Point D

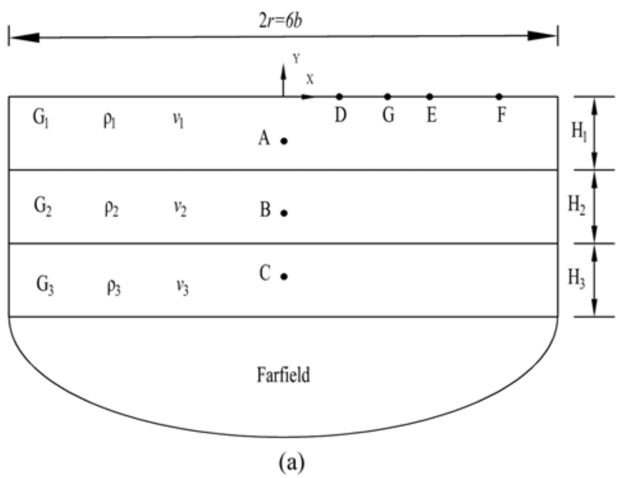

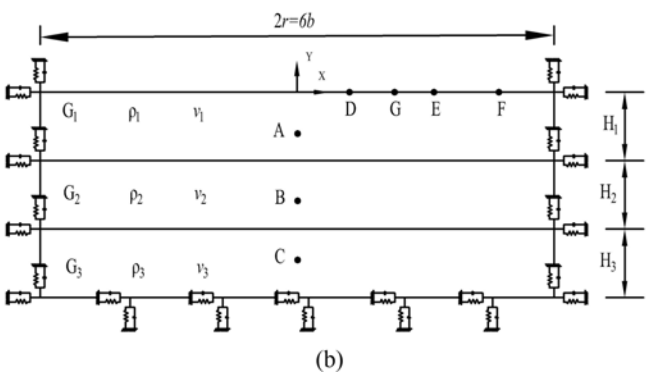

Fig. 7. The Layered Rubber Soil Foundation: (a) Calculation Diagram of the Layered Rubber Soil Foundation, (b) Viscoelastic Boundary of Layered Rubber Soil Model

method is an effective method to model the radiation damping of unbounded soil.

4.2 Influence of Rubber Soil Depth on Dynamic Response

The rubber soil is widely used in engineering field. Therefore, it is meaningful to discuss the dynamic response of rubber soil. We discuss the influence of rubber soil depth on the layered foundation in this section. A layered unbounded domain with rubber soil layer is analyzed, as shown in Fig. 7. The model is divided into nearfield and farfield, respectively. The geometry sizes of bounded domain are 90 m × 15 m. The nearfield is modeled by finite element method with eight-node element, and the mesh density is 1 m × 1 m. The farfield is modeled by viscoelastic boundary, and the boundary constants are the same as section 4.1.

Table 2. Parameters of Foundation Soil

Soil type	Rubber percentage (%)	Mass density ρ (kg/cm^3)	Elastic modulus E (MPa)	Poisson's ratio μ
Rubber soil	20	1400	5.77	0.4792
Ordinary clay	0	2100	20.45	0.3636

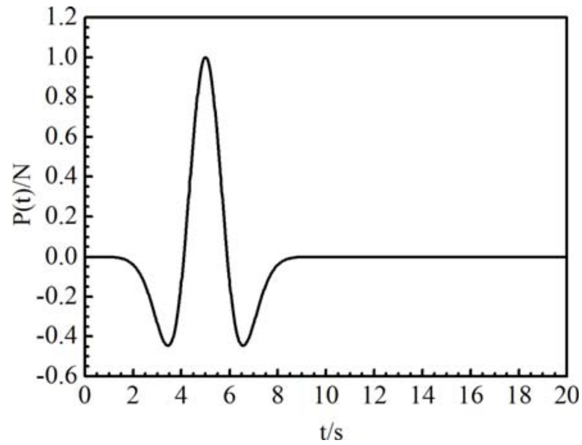

Fig. 8. Force History of Ricker Wavelet

Table 3. Observation Point Coordinate

Node	A	B	C	D	E	F	G
Coordinate	(0,-2)	(0,-7)	(0,-12)	(10,0)	(20,0)	(30,0)	(15,0)

The soil material properties are listed in Table 2. The model physical dimensions are given as: the layer thickness $h_1 = h_2 = h_3 = 5$ m. As shown in Fig. 8, the vertical Ricker wavelet force pulse $P(t)$ acts on point A. The force expressions in the time domain and frequency domain are as follow:

$$P(\mathrm{t}) = P_0\left(1-2\left(\frac{t-t_s}{t_0}\right)^2\right)\exp\left(-\left(\frac{t-t_s}{t_0}\right)^2\right), \tag{67}$$

$$P(\omega) = 0.5\sqrt{\pi}P_0 t_0(\omega t_0)^2 e^{-0.25(\omega t_0)^2}, \tag{68}$$

where $t_s = 5$, $t_0 = 4/\pi$, $P_0 = 1$.

In order to illustrate the influence of rubber soil depth on vertical displacement, three different buried depth cases are considered. According to the position of rubber soil layer, three cases are selected as: case 1: rubber soil in the first layer, case 2: rubber soil in the second layer, case 3: rubber soil in the third layer. The other soil layers are homogeneous clay soil. The material parameters are the same as those in section 4.1. In Table 3, seven observation points are selected to discuss the dynamic responses of rubber soil.

The vertical displacements of points A and G with different rubber soil depths are evaluated in Fig. 9. It can be observed from Fig. 10 that the influence of the rubber soil depth on the vertical displacement are great significant. It is clearly shown that the vertical displacement amplitudes have the following relationship: case 1 < case 3 < case 2. The displacement amplitude of case 1 is slightly less than case 3, and case 2 is the most unfavorable buried depth case. Therefore, case 1 is the optimum buried depth case for rubber soil.

The vertical displacements of the vertical and horizontal points are shown in Figs. 10 – 12. Comparing the vertical point displacements (Figs. 10(a) – 12(a)), we can notice that rubber

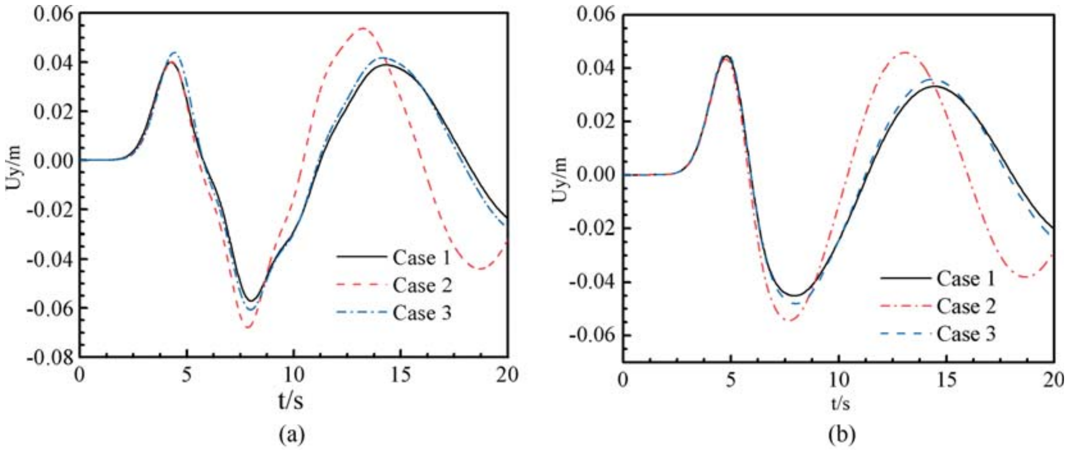

Fig. 9. Influence of the Buried Depth of Rubber Soil on Vertical Displacements: (a) Point A, (b) Point G

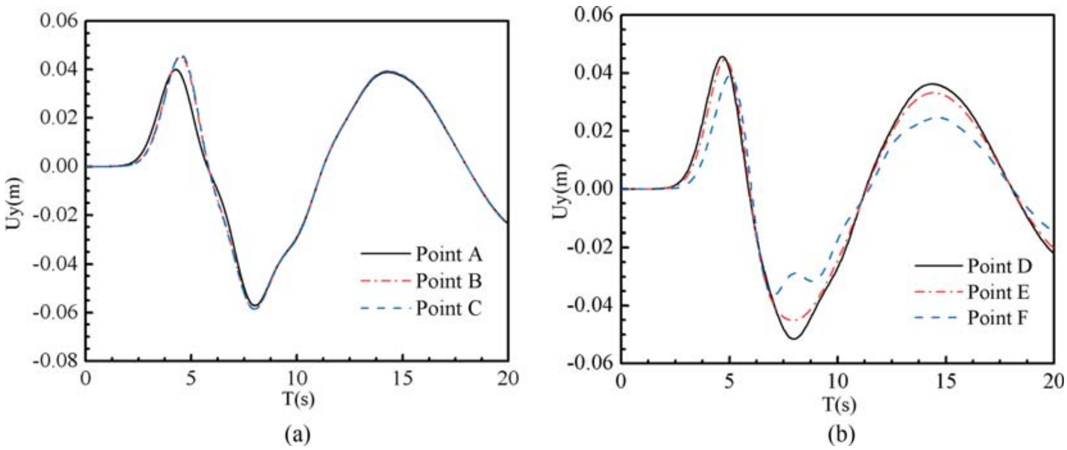

Fig. 10. Vertical Displacements of Points (case 1): (a) Vertical Points, (b) Horizontal Points

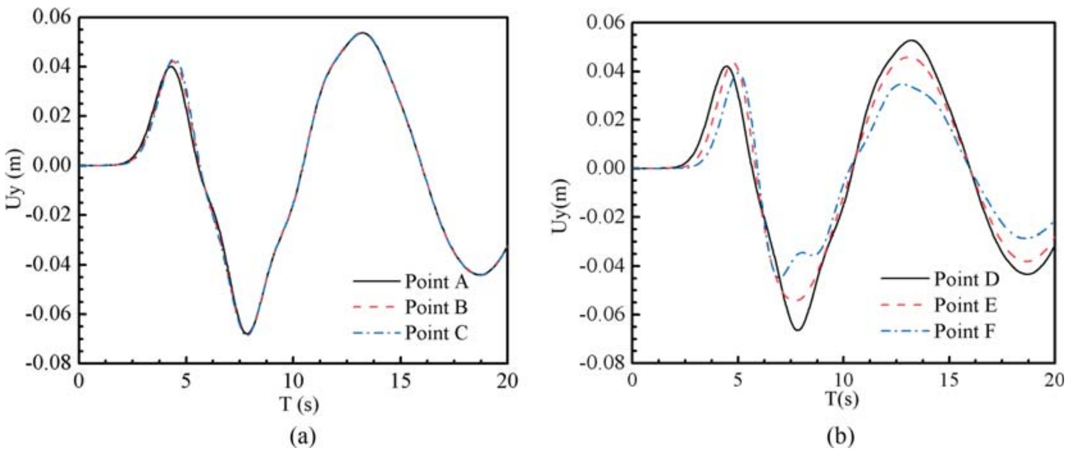

Fig. 11. Vertical Displacements of Points (case 2): (a) Vertical Points, (b) Horizontal Points

soil depth has no significant influence on the vertical displacement of the vertical points with different cases. From Figs. 10(b) – 12(b), it is observed that the horizontal distance to load point has obvious influence on displacements. When the horizontal distance increases, the vertical displacement amplitudes decrease. The displacement amplitudes change with the force, and the peak values of the displacement and force appears the same time period. The reason of this phenomenon is that the horizontal distance increases lead to the wave energy dissipation obviously.

4.3 Earthquake Response of the Layered Rubber Soil Foundation

The structural seismic performance can be improved significantly by applying seismic isolation technology. The seismic isolation

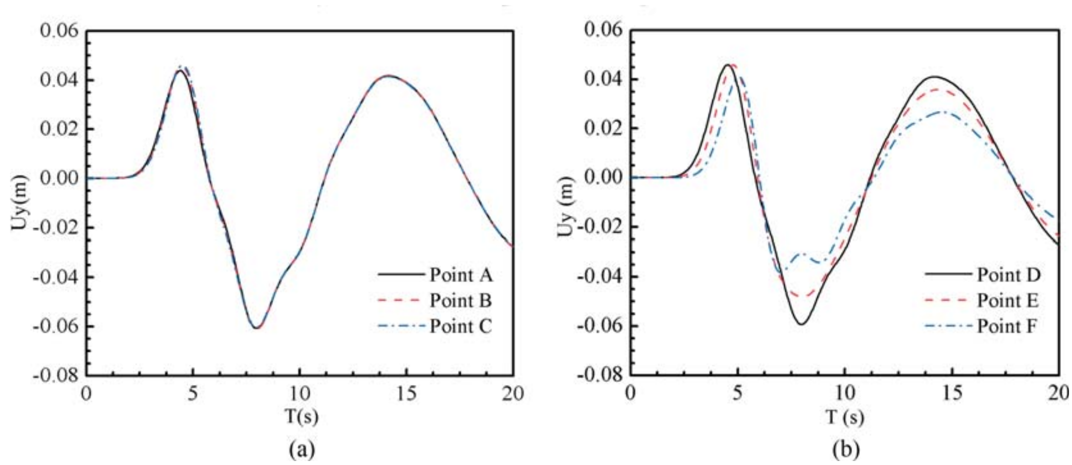

Fig. 12. Vertical Displacements of Points (case 3): (a) Vertical Points, (b) Horizontal Points

Table 4. Dynamic Calculation Parameters

K_1	K_2	n	u
30.3	1728.5	0.64	0.33

Table 5. Material Parameters of the Dam and Layered Foundation

Material type	Density ρ (kg/cm^3)	Elastic modulus E (MPa)	Possion ratio μ
Concrete	2450	42.00	0.1670
Rubber soil	1400	5.77	0.4792
Clay 1	2100	7.00	0.2500
Clay 2	2100	7.50	0.2500
Clay 3	2100	8.00	0.2500
Clay 4	2100	8.50	0.2500
Clay 5	2100	9.00	0.2500

system is implemented by setting up an isolation layer between the foundation and upper structural. Compared with the other soils, the rubber soil has high energy absorption characteristics. It can dissipate the seismic wave energy. The deformation of upper structure can be reduced significantly. Therefore, the rubber soil and structure interaction model is selected to study the seismic dynamic properties. In this section, a more severe example is performed by applying the boundaries. A simplified soil model is selected. The mechanical parameters of soil include the followings: the shear modulus, mass density, poisson ratio, hysteresis damping and equivalent viscosity damping. They are assumed as constant, and the plastic deformation is not considered. In this section, the equivalent linear model is selected as the dynamic constitutive model as listed in Table 4.

The layered foundation model with the gravity dam is analyzed, as shown in Fig. 13. The unbounded domain boundary is modeled by the viscoelastic artificial boundary. The physical dimensions of dam are given as following: the height $h = 80$ m, the width of dam top $L_1 = 20$ m, the width of dam bottom $L_2 = 60$ m. The width of bounded domain is defined as $2r = 360$ m. As shown in Fig. 13, the physical dimension of the model are given as: $h_1 = 5$ m, $h_2 = 140$ m. The physical dimensions of dam corridor are described in Fig.

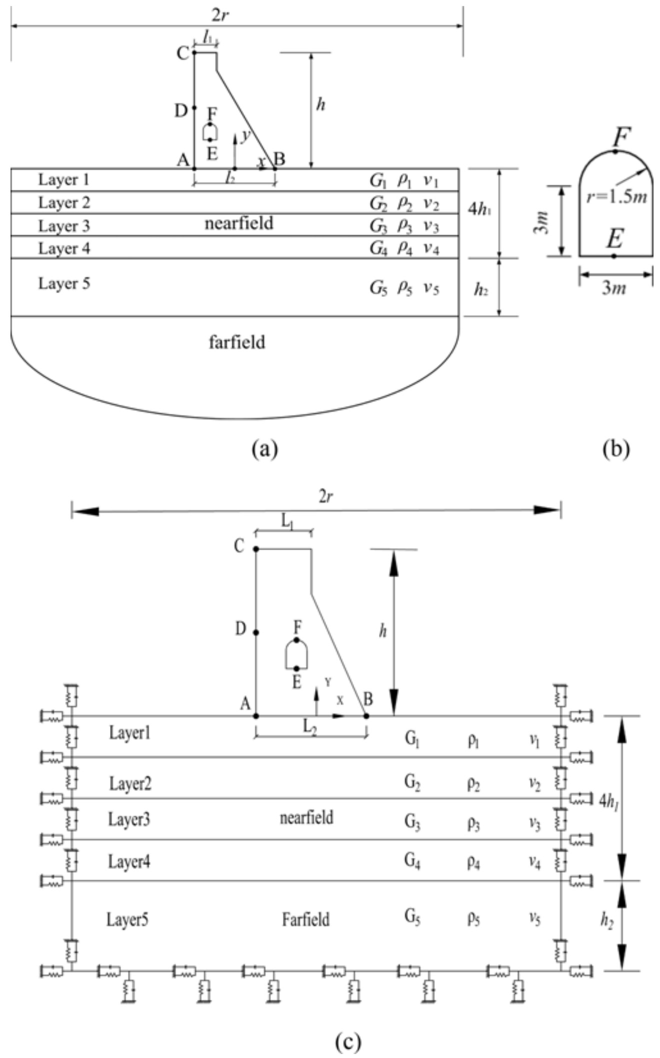

Fig. 13. The Interaction Model of Rubber Soil Foundation and Dam: (a) Rubber Soil Foundation and Dam Model, (b) Corridor Model, (c) Viscoelastic Boundary of Rubber Soil and Dam Model

Table 6. The Soil Distribution of Model

Case	Case 1 Clay soil foundation	Case 2 Rubber soil foundation
Layer 1	Clay 1	Clay 1
Layer 2	Clay 2	Rubber soil
Layer 3	Clay 3	Clay 3
Layer 4	Clay 4	Clay 4
Layer 5	Clay 5	Clay 5

13(b). The model material parameters are listed in Table 5, and the rubber proportion in rubber soil is 20%. The coordinates of observation points are given as: A(-30 m, 0), B(30 m, 0), C(-30 m, 80 m), D(-30 m, 40 m), F(-25 m, -10 m) and E(-25 m, -14.5 m).

The input displacement and velocity of the seismic wave are shown in Fig. 14. The normal boundary parameter in plane is α_n = 2.0, and the shear boundary parameter out-of plane α_t = 2.0. The time step Δt is chosen as 0.01s and the total time steps are 2000. Two foundation cases are considered as: case 1: the clay soil foundation; case 2: the rubber soil foundation, the rubber soil lies on the second layer. The details soil distribution are listed in Table 6.

A comparison study has demonstrated that the rubber soil plays an important role in the structure and foundation interaction, as illustrated in Fig. 15. Comparing the vertical accelerations of dam in Figs. 15(a) to 10(b), we observe that the vertical acceleration amplitudes of rubber soil foundation are noticeably smaller than those of clay foundation. The reason of this phenomenon is that the reflection wave is weakened by rubber soil. For $0 \le t \le 5s$, there is no difference between the acceleration of two cases. This is because the reflective wave can not take effect. For $5s \le t \le 10s$, it is observed that differences between the two cases exist and the phenomenon becomes more significant as the time increases, and the acceleration of valley decays faster than that of the peak.

In order to study the impact of dam corridor in practical engineering, the accelerations of corridor are plotted as shown in Figs. 15(e) – 15(f). The acceleration amplitudes of clay and rubber soil are compared as follows. For corridor top point F: A_{clay} = 1.0487, A_{rubber} = 0.8175; A_{clay} = -1.1776, A_{rubber} = -0.8240. For corridor bottom point E: A_{clay} = 1.0046, A_{rubber} = 0.7851; A_{clay} = -1.1492, A_{rubber} = -0.8108. As we expected that the amplitude of rubber soil is smaller than clay amplitude. The main reason is that the energy of reflection wave is weakened by rubber soil. Hence, the acceleration amplitude of rubber soil tends to decay. It is very interesting to note that the rubber soil plays a very important role in the seismic analysis of soil model.

In order to analyze the seismic performance of rubber soil further, the attenuation value and rate of acceleration peaks for two type foundations are considered as follows.

$$\Delta A = A_{clay} - A_{rubber} \tag{69}$$

$$\alpha = \Delta A / A_{clay}\ , \tag{70}$$

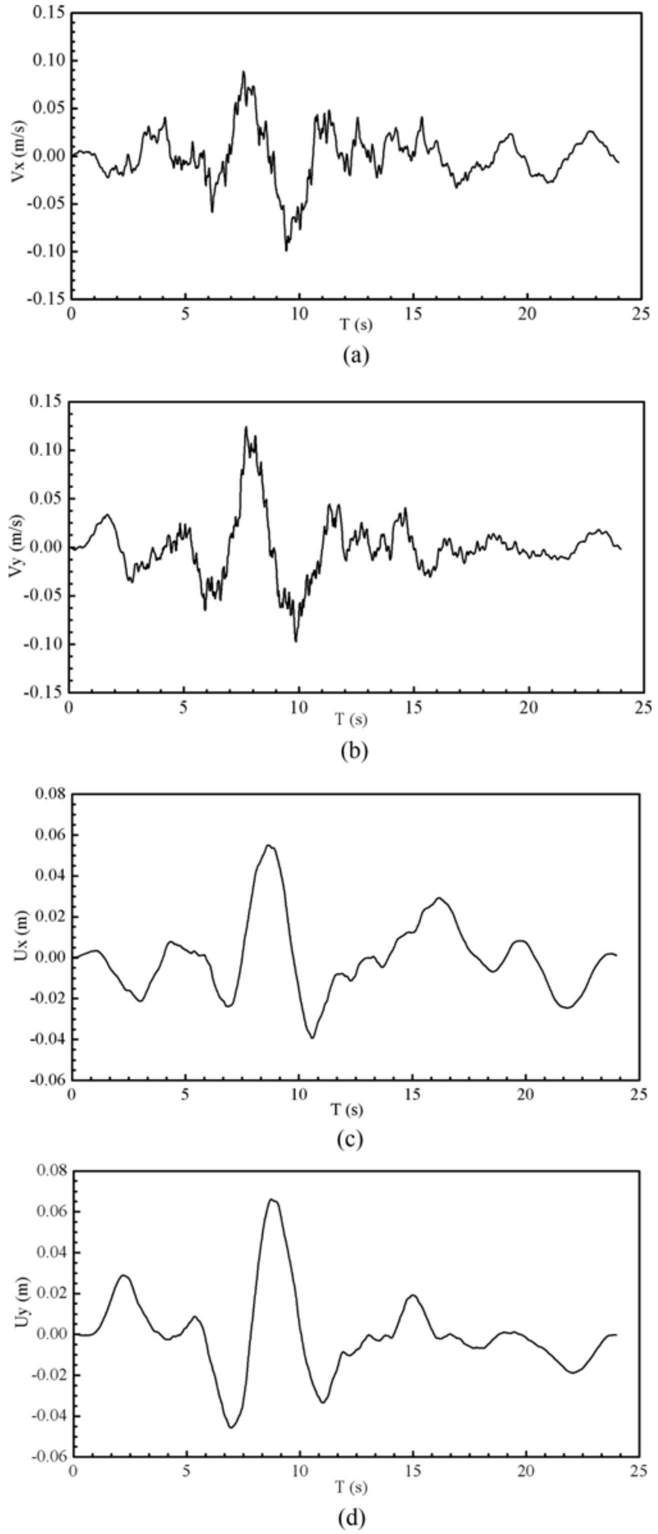

Fig. 14. The Earthquake Input for the Dam-Foundation Model: (a) The Input of Horizontal Velocity, (b) The Input of Vertical Velocity, (c) The Input of Horizontal Displacement, (d) The Input of Vertical Displacement

which ΔA is the attenuation value of acceleration peak. A_{clay} and A_{rubber} are the acceleration peak of clay and rubber soil, respectively, and α is attenuation rate. In Tables 7 and 8, the acceleration peaks

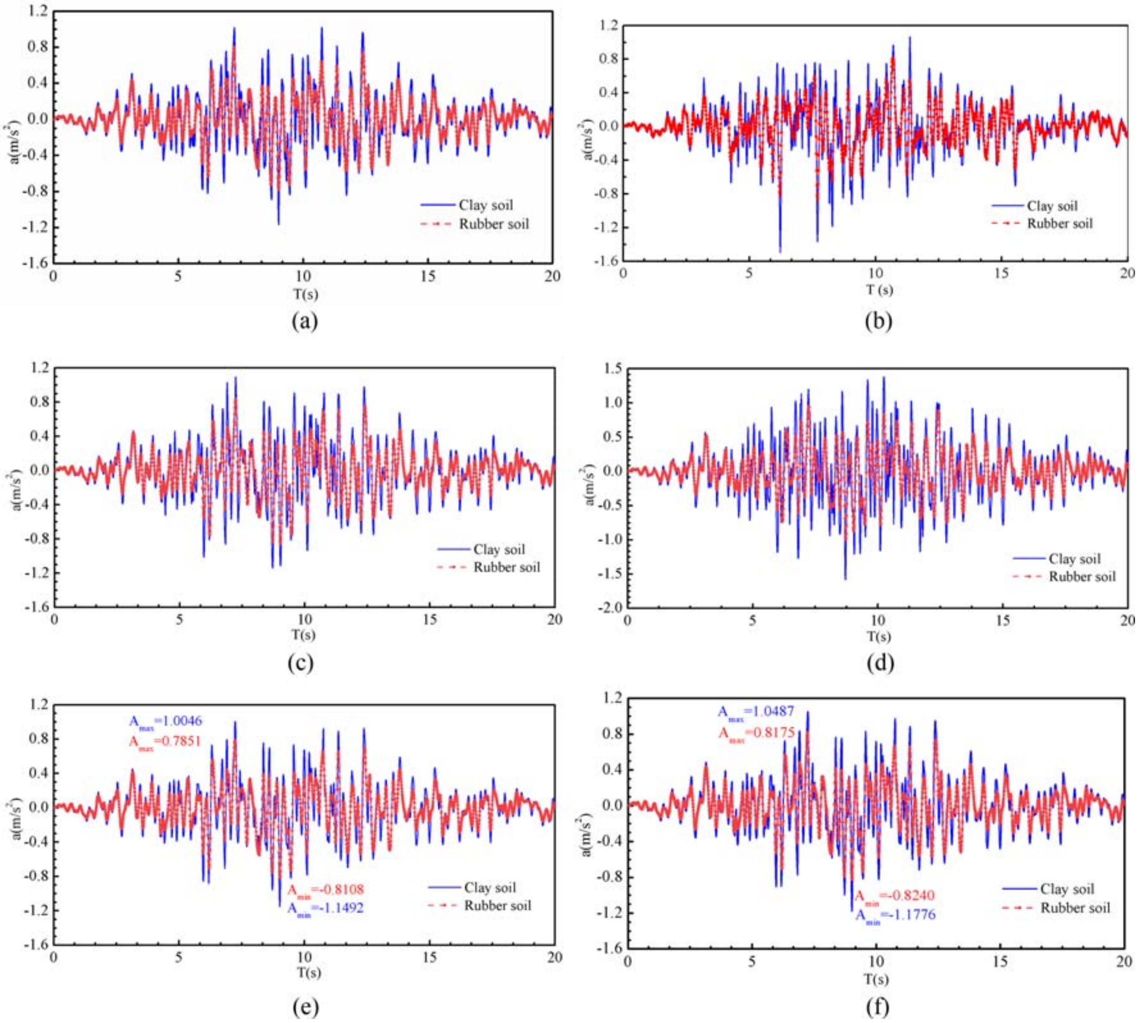

Fig. 15. Comparisons of the Vertical Acceleration: (a) Acceleration Curve of Dam Heel Point A, (b) Acceleration Curve of Dam Toe Point B, (c) Acceleration Curve of Dam Body Point D, (d) Acceleration Curve of Dam Top Point C, (e) Acceleration Curve of Point E, (f) Acceleration Curve of Point F

Table 7. Acceleration Peak of Observation Points (m/s^2)

Observation point	A	B	C	D	E	F
Rubber soil	0.803	0.812	0.951	0.837	0.785	0.817
	-0.777	-0.874	-0.992	-0.856	-0.810	-0.824
Clay	1.019	1.064	1.380	1.097	1.004	1.048
	-1.166	-1.496	-1.583	-1.140	-1.149	-1.177

Table 8. The Peak Attenuation ΔA and Attenuation Rate α

Observation point	A	B	C	D	E	F
ΔA (m/s^2)	0.39	0.62	0.59	0.28	0.34	0.35
α (%)	33.36	41.57	37.33	24.91	29.50	29.99

and its attenuation rate of observation points are listed. It is observed that the attenuation rate of dam toe (α = 41.57%) is the biggest among those points. Therefore, the rubber soil has more effect on the dynamic performance of dam toe. The main reason is that the rubber soil can reduce the reflect wave more effectively than clay. As shown in Table 7, we can observe that the highest acceleration peak occurs at the dam top point C. This is primarily due to the whipping effect in the earthquake engineering. And the acceleration peak for two cases are: A_{rubber} = -0.992 m/s^2, A_{clay} = -1.583 m/s^2. The peak of rubber soil is smaller than the peak of clay. Hence, the rubber soil has a remarkable influence on the acceleration. The rubber soil plays a very important role in the isolation system. In conclusion, rubber soil has better dynamic performance than clay. The rubber soil can play an effective role in shock absorption, and the structure-rubber soil system also has excellent seismic isolation performance.

4.4 Influence of Rubber Content on Earthquake Response

The influence of rubber content on foundation is more obvious in seismic isolation system. Hence, it is very necessary to research the influence of rubber content. The layered rubber soil model as shown in Fig. 13 is analyzed in this section. In order to consider different rubber contents, three cases are considered as: R = 10%,

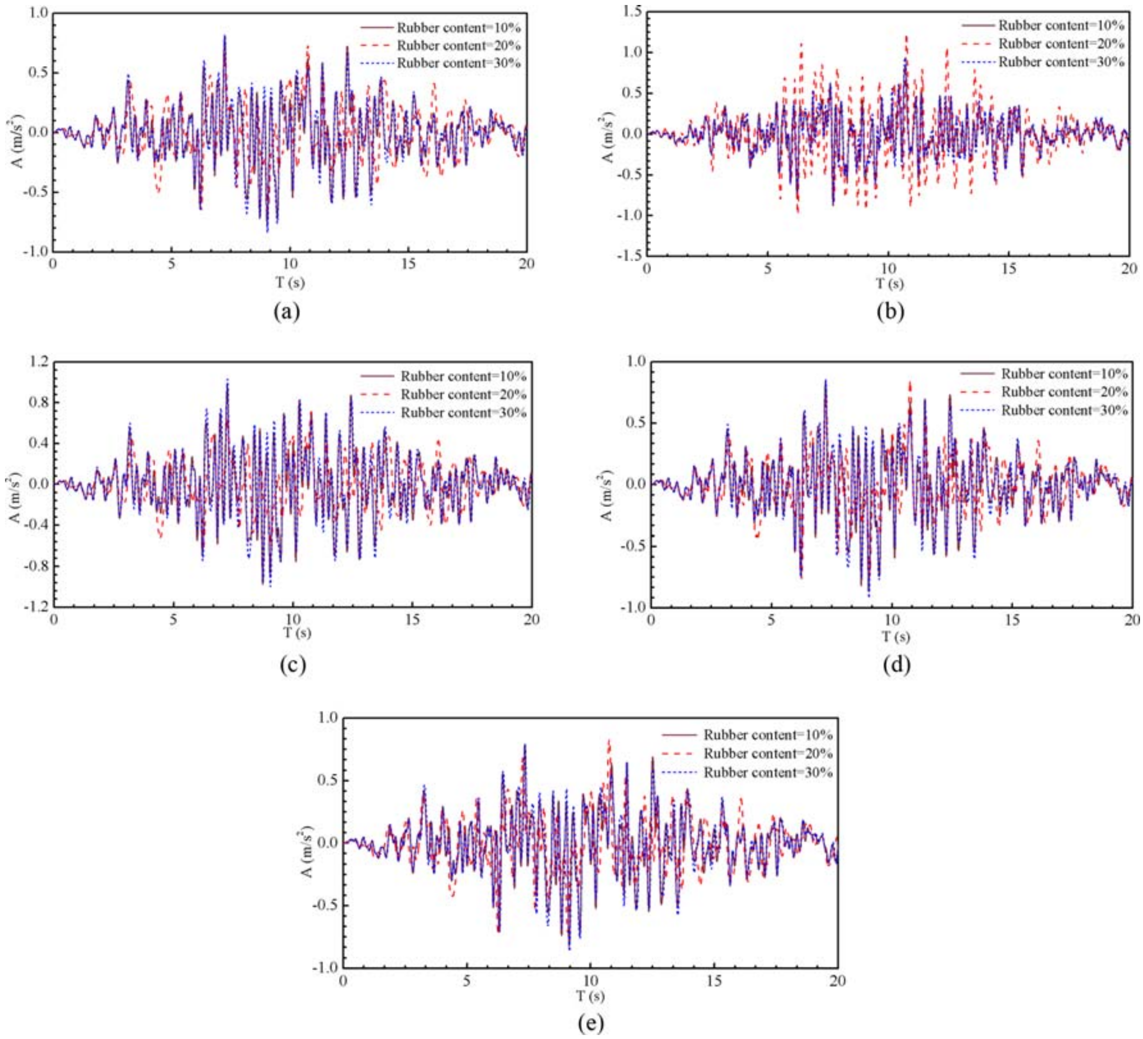

Fig. 16. The Influence of Rubber Contents: (a) Acceleration Curve of Point A, (b) Acceleration Curve of Point B, (c) Acceleration Curve of Point C, (d) Acceleration Curve of Point D, (e) Acceleration Curve of Point F

R = 20%, R = 30%. The rubber soil depth is equal to 10 m. The other parameters are the same as those of section 4.3.

As shown in Fig. 16, the vertical acceleration responses of points A, B, C, D and F with different rubber contents are plotted. It is quite obvious that the vertical accelerations are strengthened in $5s < t < 15s$. It is because that the major energy of earthquake wave occurs on this time step. When $t < 15s$, the smallest acceleration appears for the rubber content R = 20%. It is very interesting to note that the acceleration amplitude is not weakened with the increase of rubber content. On the contrary, there exists a optimal rubber content 20%. The elasticity modulus of rubber is smaller than clay. Therefore, the strength of rubber soil foundation decreases with the increase of rubber powder. For the dam heel point B, the result amplitudes of R = 10% and 30% are smaller than those of R = 20%. This is because that the closed angle of dam heel can reflect more wave for the case R = 20%. When $15s < t < 20s$, the acceleration amplitudes for R = 20% are bigger than the other two cases slightly. Overall, the rubber content R = 20% is the optimal ratio.

Table 9. Acceleration Peak of Observation Points (m/s^2)

Rubber content	A	B	C	D	E	F
0	1.166	1.496	1.583	1.140	1.149	1.177
10%	0.809	0.881	0.982	0.874	0.832	0.841
20%	0.730	1.246	0.712	0.850	0.831	0.780
30%	0.842	0.943	1.038	0.925	0.869	0.895

For the sake of comparing the rubber content influence, the acceleration amplitudes are listed in Table 9. It is clearly shown that the acceleration amplitudes with R = 20% are significantly smaller than the other two cases. To further reveal the excellent performance of rubber soil, the acceleration attenuation value ΔA and attenuation rate α are given in Tables 10 and 11 respectively. Comparing with the clay model, the acceleration attenuation rates of rubber soil model are increased significantly. For R = 10% and R = 30%, the maximal attenuation rates α occur on dam toe point B, and the values are: $\alpha_{10\%} = 41.11\%$ and $\alpha_{30\%} = 42.85\%$. For R = 20%, the maximal attenuation rate $\alpha_{20\%} = 59.44\%$

Table 10. The Peak Attenuation Value ΔA (m/s^2)

Rubber content	A	B	C	D	E	F
10%	0.374	0.615	0.601	0.266	0.320	0.336
20%	0.499	0.499	0.941	0.380	0.415	0.466
30%	0.324	0.641	0.580	0.215	0.280	0.282

Table 11. The Peak Attenuation Rate α (%)

Rubber content	A	B	C	D	E	F
10%	32.07	41.11	37.97	23.33	27.85	28.55
20%	44.43	33.36	59.44	33.33	36.12	39.59
30%	27.79	42.85	36.64	18.86	24.37	23.96

occurs on dam top point C. The significant earthquake response occurs on dam top in the actual project. This indicates that the rubber soil can reduce vibration. Therefore, the optimal rubber content is R = 20%. In summary, the rubber content increase can effectively decrease the vertical acceleration. When the rubber content is less than 20%, the wave absorption effect is obvious. When the rubber content is more than 20%, this effect tends to worse.

Table 12. Rubber-Soil Foundation Thickness

Case	H_1/m	H_2/m	H_3/m	H_4/m	H_5/m
Case 1	5	5	5	5	140
Case 2	5	10	5	5	135
Case 3	5	15	5	5	130

4.5 Influence of Rubber Soil Thickness on Earthquake Response

The earthquake response of rubber soil can be affected by soil thickness significantly. Hence, it is very necessary to research the earthquake response of rubber soil with different thicknesses. In this section, the layered rubber soil model as shown in Fig. 13 is analyzed. The seconded layer is rubber soil, and its rubber content is R = 20%. Three different thicknesses of rubber soil are

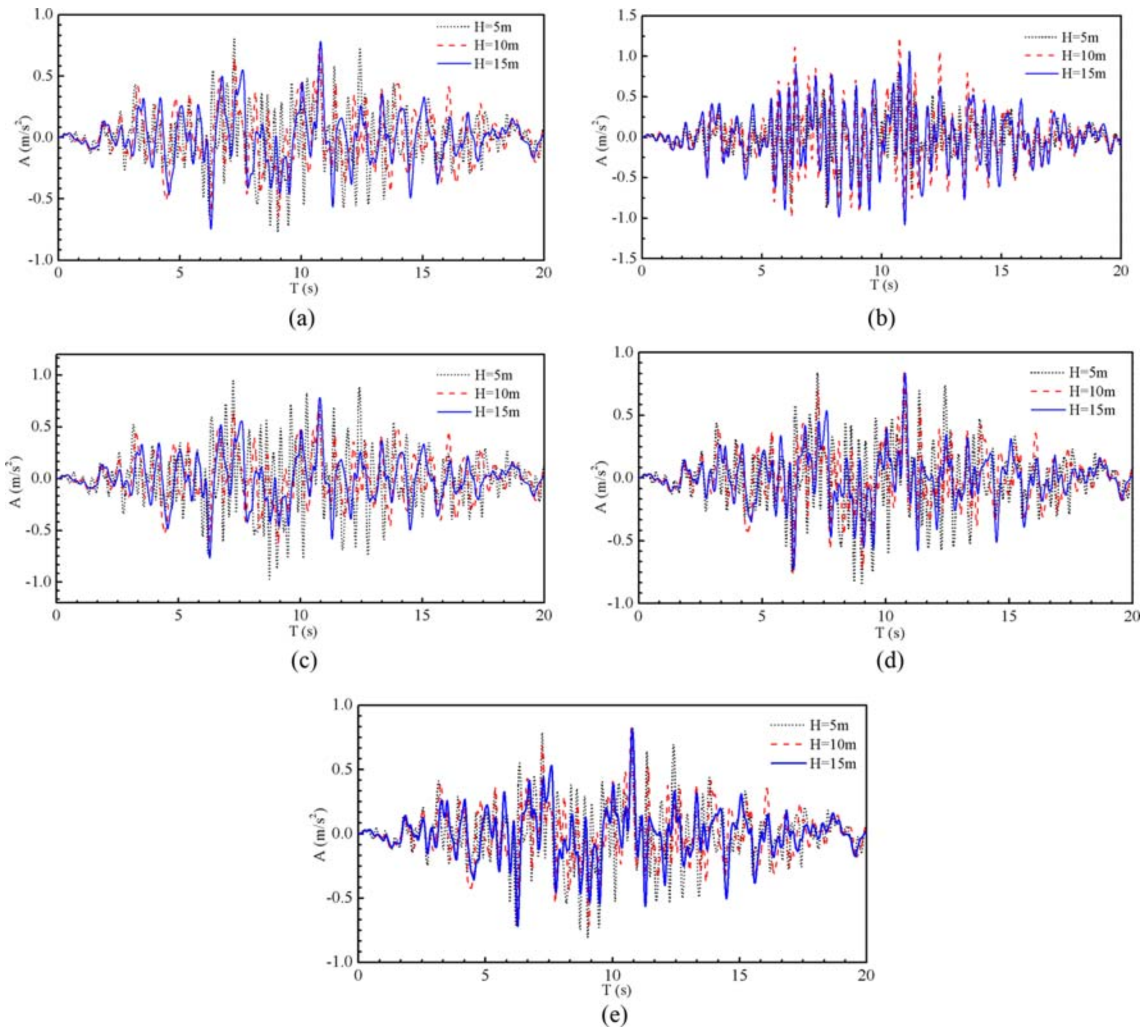

Fig. 17. The Influence of Rubber Soil Thickness: (a) Acceleration Curve of Point A, (b) Acceleration Curve of Point B, (c) Acceleration Curve of Point C, (d) Acceleration Curve of Point D, (e) Acceleration Curve of Point F

considered as: case 1: H_2 = 5 m, case 2: H_2 = 10 m, case 3: H_2 = 15 m, and the detailed soil layer thicknesses are listed in Table 12. The other parameters are the same as section 4.3.

The vertical accelerations with different rubber soil thicknesses are analyzed in Fig. 17. It can be observed from Fig. 17(a) that the accelerations of dam heel point increase first and the decrease with the rubber soil thickness increase. At last, the vertical accelerations approximately decay to zero. The maximum acceleration amplitudes occur on $5s \leq t \leq 10s$. The results of dam toe points are plotted in Fig. 17(b). From the figure, when the rubber soil thickness increase, the accelerations trend to increase first and then decrease. And the maximum amplitudes occur on $10s \leq t \leq 15s$. There is significant influence on the vertical acceleration with varying rubber soil thickness. The reason is that the bigger rubber soil thickness can reflect more wave leading to the wave overlap. It makes the difference results of dam heel and toe, and the maximum amplitudes occur to shift. However, the acceleration of dam body and top have the similar change trend as listed in Figs. 17(c) and 17(d). The acceleration decrease with the rubber soil thickness increase. It can be observed that the accelerations of dam top and body appear in a obvious negative correlation with the rubber soil thickness. As shown in Fig. 17(e), the tunnel accelerations are smaller than those of dam body. The reason is that the tunnel can reduce the wave propagation effectively.

In order to obtain the optimum rubber soil thickness, the acceleration peak, attenuation value and attenuation rate are listed in Tables 13 to 15, respectively. The peak attenuation value ΔA of rubber soil are expressed in Table 14. For the rubber soil thickness H_2 = 5 m, the peak attenuation of dam heel point B is ΔA = 0.389. It is the smallest one among three thickness cases. The conclusion can be obtained that the decay effect of dam heel decreases with rubber soil thickness increase. For the rubber soil thickness H_2 = 10 m, the peak attenuations of dam heel, dam top and tunnel points are: ΔA = 0.518, ΔA = 0.941 and ΔA = 0.466, respectively. As shown in Table 14, it can be noted that the maximum ΔA occurs on case 2 (H_2 = 10 m). For the dam body and tunnel bottom points (D and E), the biggest peak attenuations (ΔA = 0.407, ΔA = 0.430) occur on case 3 (H_2 = 15 m). As listed in Table 15, the peak attenuation rates of points D and E are: case 2: α_D = 33.33%, α_E = 36.12%; case 3: α_D = 35.70%, α_E = 37.42%. All things considered, it is evident that the results of case 2 are acceptable. For the other observation points, the results of case 2 are satisfactory. Therefore, the rubber soil thickness H_2 = 10 m is optimum, and the acceleration amplitude of dam foundation can be reduced effectively.

Table 13. Acceleration Peak of Observation Points (m/s^2)

Node	A	B	C	D	E	F
H_2 = 5 m	0.803	-0.874	-0.992	-0.856	-0.810	-0.824
H_2 = 10 m	0.730	1.246	0.712	0.850	0.831	0.780
H_2 = 15 m	0.784	-1.085	0.786	0.838	0.821	0.813
Clay soil	-1.166	-1.496	-1.583	-1.140	-1.149	-1.177

Table 14. The Peak Attenuation Value ΔA (m/s^2)

Node	A	B	C	D	E	F
H_2 = 5 m	0.389	0.622	0.591	0.284	0.339	0.353
H_2 = 10 m	0.518	0.499	0.941	0.380	0.415	0.466
H_2 = 15 m	0.418	0.411	0.819	0.407	0.430	0.441

Table 15. The Peak Attenuation Rate α (%)

Node	A	B	C	D	E	F
H_2 = 5 m	33.36	41.57	37.33	24.91	29.50	29.99
H_2 = 10 m	44.43	33.36	59.44	33.33	36.12	39.59
H_2 = 15 m	35.85	27.47	51.74	35.70	37.42	37.47

5. Conclusions

The dynamic interaction of rubber soil and structure has been analyzed in this paper. Firstly, the composite material characteristics were derived. The rubber soil was seen as a two-phase composite material which consists of rubber and soil. According to the composite material theory and hybrid law, the expression of rubber soil modulus has been derived for the first time. Then, the dynamic interaction of rubber soil and structure was discussed. Basing on the viscoelastic boundary method, the wave propagation equation of unbounded rubber soil was built. Basing on the outer wave assumptions of cylindrical expansion wave and cut-off wave, the normal and tangential boundary condition equations were derived, respectively. The earthquake response of rubber soil and structure can be solved successfully. Comparing with the other artificial boundaries, the proposed boundary can model the radiation damping of unbounded domain. It leads to the precision of proposed method be raised.

The unbounded clay soil model was analyzed first. By comparing the two reference solutions, the proposed solutions are shown to well agree with the reference solutions. It demonstrates the high accuracy and efficiency of proposed method. Subsequently, the influence of rubber soil depth on layered foundation are discussed. It can be noted that the rubber soil depth has an significant influence on the vertical displacement. This phenomenon is obvious for the buried depth 10 m case. For the buried depth 5 m case, the vertical displacement is the smallest. Therefore, the optimum buried depth is 5 m. The vertical displacement decreases with horizontal distance increases. The reason is that the increment of horizontal distance leads to the energy dissipation of wave.

Whereafter, the earthquake response of dam foundation model was further investigated. The results show that the rubber soil has excellent isolation performance. The vertical acceleration amplitudes of rubber soil are smaller than those of clay soil. The main reason for this phenomenon is that the reflection wave is weaken by rubber soil. The results show that the seismic performance of rubber soil was well. Then, the acceleration peaks and attenuation rate are discussed. Comparing with the clay soil, the rubber soil can reduce the attenuation rate effectively. Results reveal that the attenuation rate of dam toe is the biggest. It can be noticed that the rubber soil has significant influence on the dynamic performance of dam toe. So, the rubber soil can play effective role in shock absorption. Then, the influence of rubber content is discussed. The rubber content increment can effectively reduce the vertical acceleration amplitude. It confirms that the rubber soil has better shock absorption effect. The optimal rubber ratio is 20%. Last, the rubber soil thickness as another important influence factor is considered. The acceleration increases initially, and then it weakens with the thickness increase. The reason is that the increase of rubber soil thickness leads to waves overlap phenomenon. When the rubber soil thickness is 10 m, the dam acceleration amplitude can be reduced effectively.

As mentioned above, the rubber soil reveals excellent isolation performance. Because of the rubber soil owning absorbing energy characteristics, the seismic response of upper structure can be reduced effectively. The numerical solutions in this paper can provide reference for the large-scale engineering design. In the future study, the proposed new technique can be extended to the earthquake analysis of 3D layered rubber soil. It can also be applied to the slope protection engineering, the pavement and rubber soil interaction problem.

Acknowledgments

This research was supported by Key Laboratory of Environment Controlled Aquaculture (Dalian Ocean University) Ministry of Education (202305) and Science Research Funding Project of education department of Liaoning Province in 2023 (JYTMS20230482, JYTMS20230506) for which the authors are grateful.

ORCID

Not Applicable

References

Abdulrasool AS, Fattah MY, Salim NM (2020) Application of energy absorbing layer to soil-structure interaction analysis. *IOP Conference Series: Materials Science and Engineering. IOP Publishing* 737(1): 012097, DOI: 10.1088/1757-899X/737/1/012097

Arboleda-Monsalve LG, Mercado JA, Terzic V (2020) Soil-structure interaction effects on seismic performance and earthquake-induced losses in tall buildings. *Journal of Geotechnical and Geoenvironmental Engineering* 146(5):04020028, DOI: 10.1061/(ASCE)GT.1943-5606.0002248

Bandyopadhyay S, Sengupta A, Reddy GR (2015) Performance of sand and shredded rubber tire mixture as a natural base isolator for earthquake protection. *Earthquake Engineering and Engineering Vibration* 14(4):683-693, DOI: 10.1007/s11803-015-0053-y

Brunet S, de la Llera JC, Kausel E (2016) Non-linear modeling of seismic isolation systems made of recycled tire-rubber. *Soil Dynamics and Earthquake Engineering* 85:134-145, DOI: 10.1016/j.soildyn.2016.03.019

Dhanya JS, Boominathan A, Banerjee S (2020) Response of low-rise building with geotechnical seismic isolation system. *Soil Dynamics and Earthquake Engineering* 136:106187, DOI: 10.1016/j.soildyn.2020.106187

Enquan Z, Qiong W (2019) Experimental investigation on shear strength and liquefaction potential of rubber-sand mixtures. Advances in Civil Engineering, DOI: 10.1155/2019/5934961

Fakharian K, Ahmad A (2021) Effect of anisotropic consolidation and rubber content on dynamic parameters of granulated rubber-sand mixtures. *Soil Dynamics and Earthquake Engineering* 141:106531, DOI: 10.1016/j.soildyn.2020.106531

Fontara IK, Schepers W, Savidis S (2018) Finite element implementation of efficient absorbing layers for time harmonic elastodynamics of unbounded domains. *Soil Dynamics and Earthquake Engineering* 114:625-638, DOI: 10.1016/j.soildyn.2018.06.026

Jingbo L, Hui T, Xin B (2018) The seismic wave input method for soil-structure dynamic interaction analysis based on the substructure of artificial boundaries. *Chinese Journal of Theoretical and Applied Mechanics* 50(1):32-43, DOI: 10.6052/0459-1879-17-336

Josifovski J (2016) Analysis of wave propagation and soil-structure interaction using a perfectly matched layer model. *Soil Dynamics and Earthquake Engineering* 81:1-13, DOI: 10.1016/j.soildyn.2015.10.008

Li S, Liu J, Bao X (2020) Stability analysis of an explicit integration algorithm with 3d viscoelastic artificial boundary elements. *Mathematical Problems in Engineering*, 1-18, DOI: 10.1155/2020/1848169

Li ST, Liu JB, Bao X (2020) Stability analysis of explicit algorithms with visoco-elastic artificial boundary elements. *Engineering Mechanics* 37(11):1-11, 46, DOI: 10.6052/j.issn.1000-4750.2019.12.0755

Liu J, Bao X, Wang D (2019) The internal substructure method for seismic wave input in 3D dynamic soil-structure interaction analysis. *Soil Dynamics and Earthquake Engineering* 127:105847, DOI: 10.1016/j.soildyn.2019.105847

Løkke A, Chopra AK (2018) Direct finite element method for nonlinear earthquake analysis of 3-dimensional semi-unbounded dam-water-foundation rock systems. *Earthquake Engineering & Structural Dynamics* 47(5):1309-1328, DOI: 10.1002/eqe.3019

Madhusudhan BR, Boominathan A, Banerjee S (2019) Properties of sand-rubber tyre shreds mixtures for seismic isolation applications. *Soil Dynamics and Earthquake Geotechnical Engineering*. Springer, Singapore, 267-274, DOI: 10.1007/978-981-13-0562-7

Manohar DR, Anbazhagan P (2021) Shear strength characteristics of geosynthetic reinforced rubber-sand mixtures. *Geotextiles and Geomembranes* 49(4):910-920, DOI: 10.1016/j.geotexmem.2020.12.015

Moghaddas Tafreshi SN, Joz Darabi N, Tavakoli Mehrjardi G (2016) Experimental and numerical investigation of footing behaviour on multi-layered rubber-reinforced soil. *European Journal of Environmental and Civil Engineering* 23(1):29-52, DOI: 10.1080/19648189.2016.1262288

Mohajerani A, Burnett L, Smith JV (2020) Recycling waste rubber tyres in construction materials and associated environmental considerations: A review. *Resources, Conservation and Recycling* 155:104679, DOI: 10.1016/j.resconrec.2020.104679

Nanda RP, Dutta S, Khan HA (2018) Seismic protection of buildings by rubber-soil mixture as foundation isolation. *International Journal of Geotechnical Earthquake Engineering (IJGEE)* 9(1):99-109, DOI: 10.4018/IJGEE.2018010106

Olia ASR, Perić D (2021) Thermomechanical soil-structure interaction in single energy piles exhibiting reversible interface behavior. *International Journal of Geomechanics* 21(5):04021065, DOI: 10.1061/(ASCE)GM.1943-5622.0002014

Pistolas GA, Pitilakis K, Anastasiadis A (2020) A numerical investigation on the seismic isolation potential of rubber/soil mixtures. *Earthquake Engineering and Engineering Vibration* 19(3):683-704, DOI: 10.1007/s11803-020-0589-3

Pitilakis D, Anastasiadis A, Vratsikidis A (2021) Large-scale field testing of geotechnical seismic isolation of structures using gravel-rubber mixtures. *Earthquake Engineering & Structural Dynamics* 50(10):2712-2731, DOI: 10.1002/eqe.3468

Pitilakis K, Karapetrou S, Tsagdi K (2015) Numerical investigation of the seismic response of RC buildings on soil replaced with rubber-sand mixtures. *Soil Dynamics and Earthquake Engineering* 79:237-252, DOI: 10.1016/j.soildyn.2015.09.018

Rouhanifar S, Afrazi M, Fakhimi A (2020) Strength and deformation behavior of sand-rubber mixture. *International Journal of Geotechnical Engineering*, 1-15, DOI: 10.1080/19386362.2020.1812193

Sanchez JB (2020) Cyclic performance of rubber-soil mixtures to enhance seismic protection. Doctoral Dissertation, DOI: 10.17869/enu.2020.2683555

Tasalloti A, Chiaro G, Palermo A (2020) Effect of rubber crumbs volumetric content on the shear strength of gravelly soil in direct shear apparatus. *Geo-Congress 2020: Geo-Systems, Sustainability, Geoenvironmental Engineering, and Unsaturated Soil Mechanics. Reston, VA: American Society of Civil Engineers*, 259-266

Tsang HH, Pitilakis K (2019) Mechanism of geotechnical seismic isolation system: Analytical modeling. *Soil Dynamics and Earthquake Engineering* 122:171-184, DOI: 10.1016/j.soildyn.2019.03.037

Tsang HH, Tran DP, Hung WY (2021) Performance of geotechnical seismic isolation system using rubber-soil mixtures in centrifuge testing. *Earthquake Engineering & Structural Dynamics* 50(5): 1271-1289, DOI: 10.1002/eqe.3398

Tsiavos A, Alexander NA, Diambra A (2019) A sand-rubber deformable granular layer as a low-cost seismic isolation strategy in developing countries: Experimental investigation. *Soil Dynamics and Earthquake Engineering* 125:105731, DOI: 10.1016/j.soildyn.2019.105731

Wang FC (2019) Experimental study on properties of rubberized cement soil. Science Press of China (in Chinese)

Wang C, Deng A, Taheri A (2018) Three-dimensional discrete element modeling of direct shear test for granular rubber-sand. *Computers and Geotechnics* 97:204-216, DOI: 10.1016/j.compgeo.2018.01.014

Yuan B, Xiong L, Zhai L (2019) Transparent synthetic soil and its application in modeling of soil-structure interaction using optical system. *Frontiers in Earth Science* 7:276, DOI: 10.3389/feart.2019.00276

Zhang G, Zhao M, Du X (2020) A frequency-dependent absorbing boundary condition for numerically solving u-U elastic wave equations in layered and fluid-saturated porous media. *Soil Dynamics and Earthquake Engineering* 135:106189, DOI: 10.1016/j.soildyn.2020.106189

Zhao M, Li H, Du X (2019) Time-domain stability of artificial boundary condition coupled with finite element for dynamic and wave problems in unbounded media. *International Journal of Computational Methods* 16(4):1850099, DOI: 10.1142/S0219876218500998

Zhou CG (2009) Research on the mechanism of seismic wave input about high rockfilldam. Dalian University of Technology (in Chinese)